PERGAMON Mathematical and Computer Modelling 32 (2000) 323–340

MATHEMATICAL AND COMPUTER MODELLING

www.elsevier.nl/locate/mcm

A Three-Point Sixth-Order Staggered Combined Compact Difference Scheme

PETER C. CHU AND CHENWU FAN
Department of Oceanography, Naval Postgraduate School
Monterey, CA 93943, U.S.A.

(Received January 2000; accepted February 2000)

Abstract—A three-point, sixth-order, staggered, combined compact difference (SCCD) scheme is proposed for numerical models. The SCCD scheme is a generalization of the previously proposed combined compact difference (CCD) scheme, and has major improved features such as error and computational (CPU) time reduction especially for odd-order difference equations with odd-number boundary conditions. For nonperiodic boundaries, an additional sixth- or fifth-order boundary condition is proposed. The stability of the SCCD scheme is studied using the eigenvalue analysis.

Keywords—Blasius equation, Combined compact difference scheme, Computational stability, Sigma-coordinate ocean model, Staggered grid.

1. INTRODUCTION

Following the trend toward highly accurate numerical schemes of partial differential equations (PDE) led by many authors (e.g., Adam [1]; Lele [2]; Carpenter *et al.* [3,4]; Chu and Fan [5]; Hirsh [6]; Rubin and Khosla [7]; Navon and Riphagen [8], and Chu and Fan [9,10]) proposed a three-point sixth-order uniform and nonuniform combined compact difference (CCD) schemes to increase accuracy. This scheme follows earlier work on use of second derivatives in compact difference (such as [7])

$$\sum_{k=-1}^{1} \left(a_k f_{i+k} + b_k f'_{i+k} + c_k f''_{i+k}\right) = 0, \tag{1}$$

which is referred to as the Hermite formula. Here, f is a dependent variable. Lele [2] and Carpenter *et al.* [3,4] performed detailed studies of several compact schemes in terms of accuracy and efficiency, both for first- and second-order derivatives f' and f''. Moreover, Carpenter *et al.* [3] address the issue of stability of boundary stencils from the theoretical point of view.

Many ocean and atmospheric numerical models are designed on staggered grids, this is due to the fact that the staggered grids give more accurate wave propagation. Applying the CCD scheme to the staggered grids, we obtain a three-point sixth-order staggered combined compact

This work was funded by the Office of Naval Research Naval Ocean Modeling and Prediction (NOMP) program, the Naval Oceanographic Office, and the Naval Postgraduate School.

0895-7177/00/$ - see front matter Typeset by AMS-TEX
PII: S0895-7177(00)00138-2

Report Documentation Page

Form Approved
OMB No. 0704-0188

1. REPORT DATE	2. REPORT TYPE	3. DATES COVERED
FEB 2000		**00-00-2000 to 00-00-2000**

4. TITLE AND SUBTITLE	5a. CONTRACT NUMBER
A Three-Point Sixth-Order Staggered Combined Compact Difference Scheme	5b. GRANT NUMBER
	5c. PROGRAM ELEMENT NUMBER
6. AUTHOR(S)	5d. PROJECT NUMBER
	5e. TASK NUMBER
	5f. WORK UNIT NUMBER
7. PERFORMING ORGANIZATION NAME(S) AND ADDRESS(ES) **Naval Postgraduate School,Monterey ,CA,93943**	8. PERFORMING ORGANIZATION REPORT NUMBER
9. SPONSORING/MONITORING AGENCY NAME(S) AND ADDRESS(ES)	10. SPONSOR/MONITOR'S ACRONYM(S)
	11. SPONSOR/MONITOR'S REPORT NUMBER(S)

12. DISTRIBUTION/AVAILABILITY STATEMENT
Approved for public release; distribution unlimited

13. SUPPLEMENTARY NOTES

14. ABSTRACT

15. SUBJECT TERMS

16. SECURITY CLASSIFICATION OF:			17. LIMITATION OF ABSTRACT	18. NUMBER OF PAGES	19a. NAME OF RESPONSIBLE PERSON
a. REPORT **unclassified**	b. ABSTRACT **unclassified**	c. THIS PAGE **unclassified**	**Same as Report (SAR)**	**18**	

difference (SCCD) scheme with sixth-order or fifth-order accuracy at both interior and boundary points.

2. SCCD SCHEME

2.1. General Form

Let $f(x)$ be defined on the interval, $0 \leq x \leq L$. We discretize the interval into $0 = x_0 < x_1 < \cdots < x_N = L$ for nonperiodic boundaries (Figure 1a) and into $0 < x_0 < x_1 < \cdots < x_N < L$ for periodic boundaries (Figure 1b) with a grid spacing $h = x_i - x_{i-1} = L/N$, $(i = 1, 2, \ldots, N)$. Here, $x_0, x_1, \ldots, x_N$ are unstaggered points.

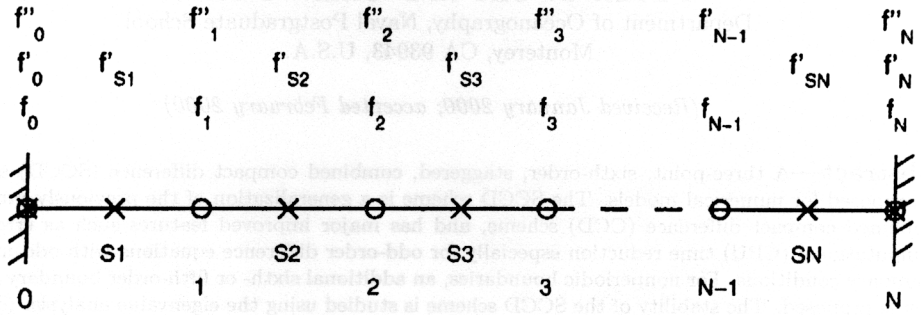

(a) Nonperiodic boundaries.

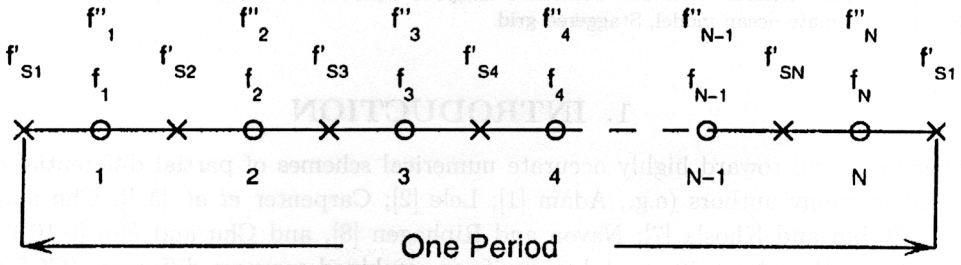

(b) Periodic boundaries.

Figure 1. Illustration of the SCCD grid structure.

Use staggered grids, $0 = x_{S0} = x_0 < x_{S1} < x_1 < \cdots < x_{SN} < x_N = x_{SN+1} = L$ for nonperiodic boundaries (Figure 1a), and $0 = x_{S1} < x_1 < x_{S2} < \cdots < x_{SN} < x_N < L$ for periodic boundaries (Figure 1b) with $x_{Si} = x_i - h/2$, $i = 1, 2, 3, \ldots, N$. Here, $x_{S1}, x_{S2}, \ldots, x_{SN}$ are staggered grid points. Notice that staggered and unstaggered points are collocated at nonperiodic boundaries ($x_{S0} = x_0$ and $x_{SN+1} = x_N$).

The dependent variable $f(x)$ and its second derivative $f''(x)$ are given at the unstaggered points. The first derivative $f'(x)$ is given at the staggered points. By application of the Hermite formula (1) to the staggered grids, we obtain a general form of the SCCD scheme

$$\alpha_{11} f'_{Si-1} + f'_{Si} + \alpha_{12} f'_{i+1} + \beta_{11} f''_{i-1} + \beta_{12} f''_i = \gamma_1 (f_i - f_{i-1}), \tag{2}$$

$$\alpha_{21} f'_{Si} + \alpha_{22} f'_{Si+1} + \beta_{21} f''_{i-1} + f''_i + \beta_{22} f''_{i+1} = \gamma_{21} f_{i-1} - (\gamma_{21} + \gamma_{22}) f_i + \gamma_{22} f_{i+1}. \tag{3}$$

In computing first and second derivatives, systems (2) and (3) will be solved for unknown variables f' and f'' as f is given at the regular grids f_{i-1}, f_i, and f_{i+1}. The coefficients in (2) and (3) are determined by the Taylor series expansion.

2.2. Expansion on Staggered Grid Points

2.2.1. General expressions

Expansion of f, f', and f'' into the Taylor series at the staggered grids x_{Si} and elimination of h^2 and h^4 terms leads to (Figure 2a)

$$f'_{Si} - \frac{7}{254}\left(f'_{Si-1} + f'_{Si+1}\right) + \frac{17h}{254}\left(f''_i - f''_{i-1}\right) = \frac{120}{127h}\left(f_i - f_{i-1}\right) \tag{4}$$

with truncation error $-1/(7!)(457/2032)f^{(7)}_{Si}h^6$. Using a similar procedure expansion, we also can obtain

$$f_{Si} = \frac{1}{2}\left(f_i + f_{i-1}\right) + \frac{5}{32}h\left(f'_{Si+1} - f'_{Si-1}\right) - \frac{7}{32}h^2\left(f''_i + f''_{i-1}\right), \tag{5}$$

with truncation error $-1/(6!)(137/2^7)f^{(6)}_{Si}h^6$.

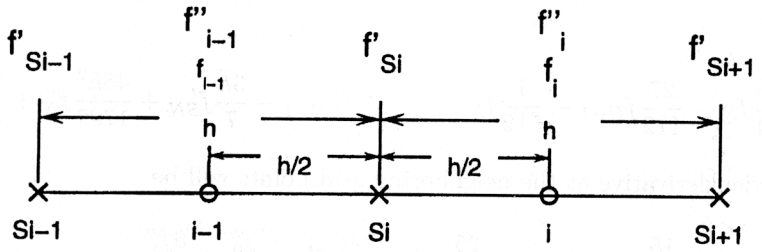

(a) Staggered grid points.

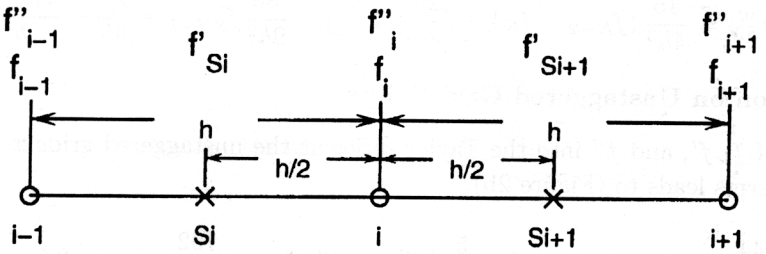

(b) Standard grid points.

Figure 2. Illustration of the SCCD grid structure at interior.

In some cases, if the third-order derivative is required, a similar formulation will be

$$f'''_{Si} = -\frac{120}{127h^2}\left(f'_{Si-1} + f'_{Si+1}\right) + \frac{237}{127h}\left(f''_i - f''_{i-1}\right) + \frac{240}{127h^3}\left(f_i - f_{i-1}\right). \tag{6}$$

Expressions (4)–(6) are valid from x_{S1} to x_{SN} for the periodic boundaries, and from x_{S2} to x_{SN-1} for the nonperiodic boundaries. Thus, each of (4)–(6) contains N algebraic equations for the periodic boundaries and $(N-2)$ algebraic equations for the nonperiodic boundaries.

2.2.2. Special expressions for nonperiodic boundaries

Expansion of f, f', and f'' into the Taylor series at grids x_{S1} from neighboring points and elimination of h^2 and h^4 terms lead to (Figure 3)

$$\frac{7}{135}f'_0 + \frac{32}{25}f'_{S1} - \frac{224}{675}f'_{S2} - \frac{h}{45}f''_0 + \frac{6h}{25}f''_1 = -\frac{57}{50h}f_0 + \frac{32f_1}{25h} - \frac{7}{50h}f_2 \tag{7}$$

for the left boundary with the truncation error as $1/(7!)(2/5)f^{(7)}_{S1}h^6$. Similarly, we have

$$\frac{7}{135}f'_N + \frac{32}{25}f'_{SN} - \frac{224}{675}f'_{SN-1} + \frac{h}{45}f''_N - \frac{6h}{25}f''_{N-1} = \frac{57}{50h}f_N - \frac{32f_{N-1}}{25h} + \frac{7}{50h}f_{N-2} \tag{8}$$

for the right boundary with the same order of the truncation error.

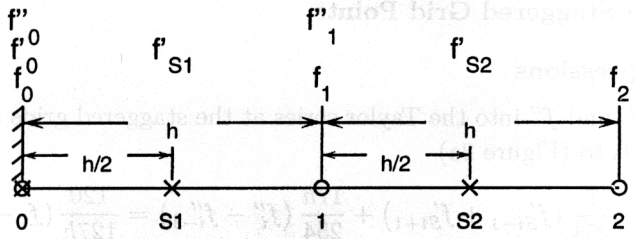

Figure 3. Illustration of the SCCD grid structure at the left boundary.

Besides, the sixth-order interpolation near the boundary staggered grid points are

$$f_{S1} = \frac{4455}{3584} f_0 - \frac{27}{112} f_1 - \frac{1}{512} f_2 + \frac{81}{256} f'_0 + \frac{3}{7} f'_{S1} + \frac{45}{1792} f''_0 + \frac{9}{896} f''_1 \tag{9}$$

and

$$f_{SN} = \frac{4455}{3584} f_N - \frac{27}{112} f_{N-1} - \frac{1}{512} f_{N-2} - \frac{81h}{256} f'_{SN+1} - \frac{3h}{7} f'_{SN} + \frac{45h^2}{1792} f''_N + \frac{9h^2}{896} f''_{N-1}. \tag{10}$$

The third-order derivative at the neighboring grid points will be

$$f'''_{S1} = \frac{15}{4h^3}(f_2 - f_0) + \frac{25}{18h^2} f'_0 - \frac{80}{9h^2} f'_{S2} - \frac{f''_0}{6h} + \frac{6f''_1}{h}, \tag{11}$$

$$f'''_{SN} = \frac{15}{4h^3}(f_{N-2} - f_N) + \frac{25}{18h^2} f'_{SN+1} - \frac{80}{9h^2} f'_{SN-1} + \frac{f''_N}{6h} - \frac{6f''_{N-1}}{h}. \tag{12}$$

2.3. Expansion on Unstaggered Grid Points

Expansion of f, f', and f'' into the Taylor series at the unstaggered grids x_i and elimination of h^2 and h^4 terms leads to (Figure 2b)

$$-\frac{144}{47h}(f'_{Si+1} - f'_{Si}) + f''_i - \frac{5}{94}(f''_{i-1} + f''_{i+1}) = -\frac{102}{47h^2}(f_{i-1} - 2f_i + f_{i+1}) \tag{13}$$

with truncation error $-1/(7!)(1/4) f^{(8)}(x_i) h^6$. Expression (13) is valid from x_1 to x_N for the periodic boundaries, and from x_1 to x_{N-1} for the nonperiodic boundaries. Thus, equation (13) contains N algebraic equations for the periodic boundaries and $(N-1)$ algebraic equations for the nonperiodic boundaries.

2.4. Periodic Boundaries

For periodic boundaries

$$f_0 = f_N, \quad f_{N+1} = f_1, \quad f'_{S0} = f'_{SN}, \quad f'_{SN+1} = f'_{S1}, \quad f''_0 = f''_N, \quad \text{and} \quad f''_{N+1} = f''_1, \tag{14}$$

the SCCD scheme (4) and (13) automatically provide the sixth-order accuracy for whole region (interior and boundary points).

3. ALGORITHM FOR NONPERIODIC BOUNDARIES

Treatment for nonperiodic boundaries is an important task for the high-order schemes. Following Carpenter *et al.* [11], Chu and Fan [9,10] proposed a boundary treatment for the three-point sixth-order unstaggered CCD schemes. Here, we propose a fifth-order boundary algorithm for SCCD scheme.

3.1. Finite Difference Equation (FDE)

Consider a one-dimensional Euler equation

$$\frac{\partial f}{\partial t} + c\frac{\partial f}{\partial x} = d, \qquad 0 \le x \le L, \quad 0 \le t \tag{15}$$

with the initial and boundary conditions

$$f(0,x) = g(x), \qquad f(t,0) = p(t). \tag{16}$$

Use of the SCCD scheme (5), (9), and (10) leads to the discretization

$$\frac{\Delta f_{Si}}{\Delta t} + c f'_{Si} = d, \qquad i = 0,1,\ldots,N+1, \tag{17}$$

which contains $(N+2)$ algebraic equations.

There are $(3N+4)$ unknown variables in this system: $f_i\,(i=0,\ 1,\ldots,N)$, $f'_{Si}\,(i=0,\ 1,2,\ldots,N+1)$, and $f''_i(i=0,\ 1,\ldots,N)$, however, only $(3N+2)$ algebraic equations are available in (4), (7), (8), (13), and (17). We need two more algebraic equations to close the system. The two additional boundary conditions for the SCCD scheme are (Figure 3)

$$f'_0 + \frac{128}{7}f'_{S1} - \frac{3h}{7}f''_0 + \frac{10h}{7}f''_1 = \frac{128}{7h}(f_1 - f_0) + \frac{1}{2h}(f_2 - f_0), \tag{18}$$

$$f'_N + \frac{128}{7}f'_{SN} + \frac{3h}{7}f''_N - \frac{10h}{7}f''_{N-1} = -\frac{128}{7h}(f_{N-1} - f_N) - \frac{1}{2h}(f_{N-2} - f_N) \tag{19}$$

with a fifth-order truncation error, $-1/(180)f_1^{(6)}h^5$, for the left and right boundaries, respectively. The coefficient matrix is a diagonal system with eight bands when nonperiodic (Figure 4) and with seven bands when periodic (Figure 5). Thus, the memory requirement is $8(3N+4)$ when nonperiodic and $7(3N+4)$ when periodic.

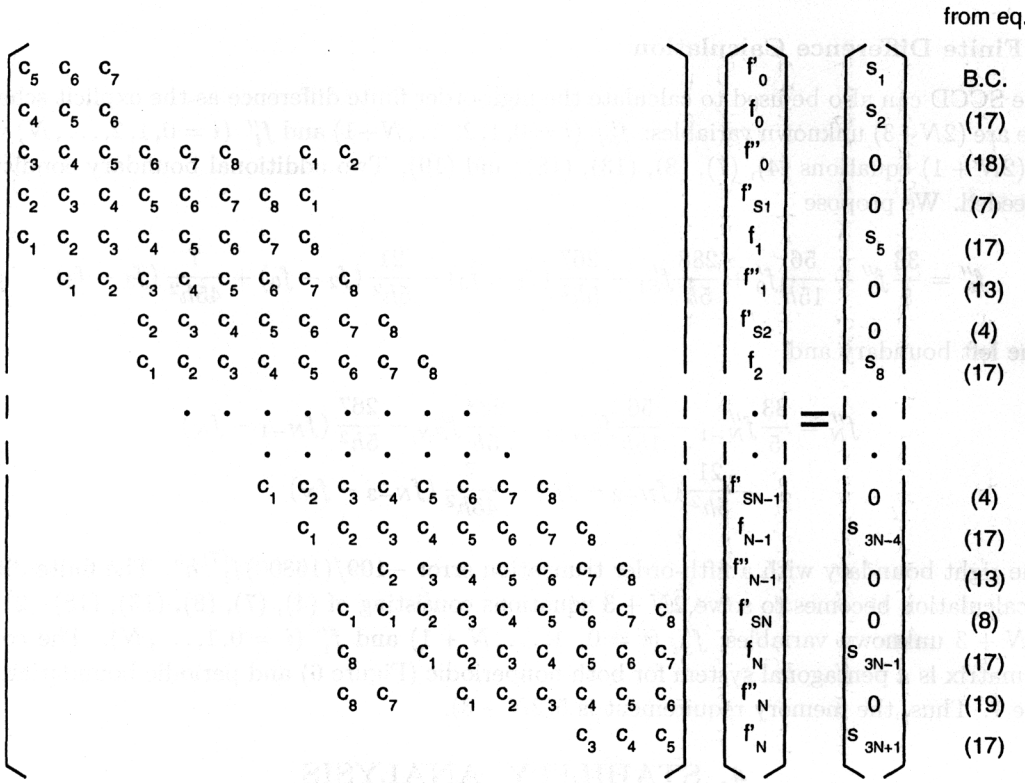

Figure 4. Coefficient matrix of the SCCD scheme for finite difference calculation with nonperiodic boundaries.

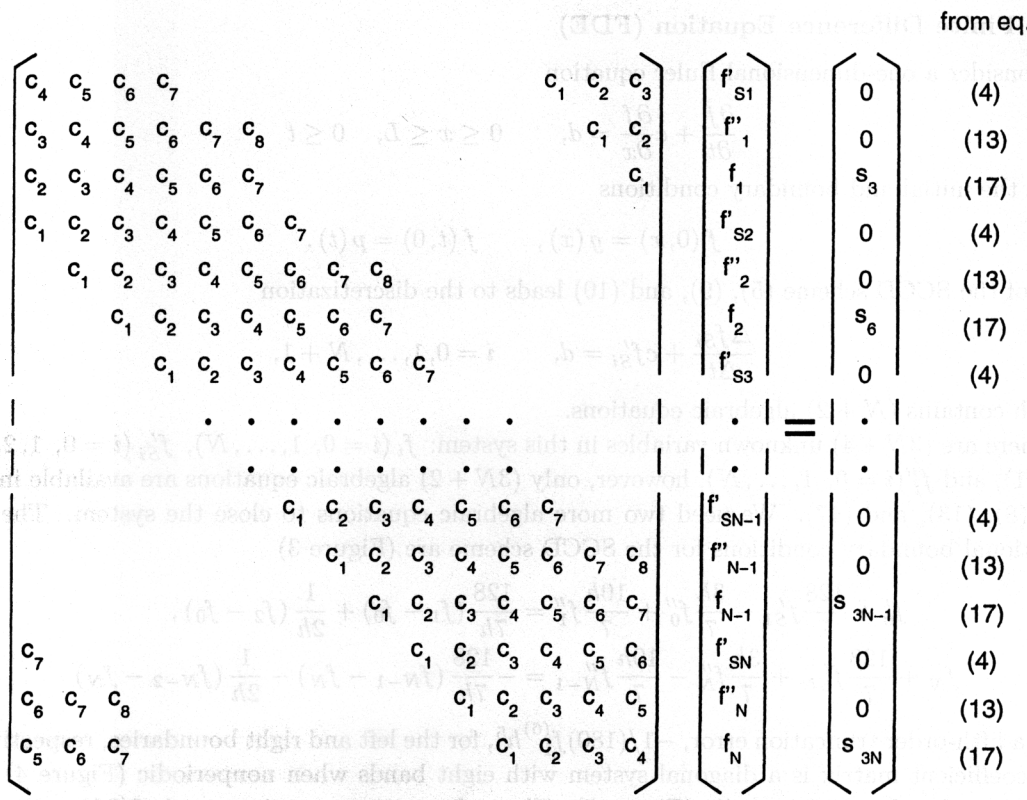

Figure 5. Coefficient matrix of the SCCD scheme for finite difference calculation with periodic boundaries.

3.2. Finite Difference Calculation

The SCCD can also be used to calculate the high-order finite difference as the explicit scheme. There are $(2N+3)$ unknown variables: f'_{Si} $(i = 0, 1, 2, \ldots, N+1)$ and f''_i $(i = 0, 1, 2, \ldots, N)$ with only $(2N + 1)$ equations (4), (7), (8), (13), (18), and (19). Two additional boundary conditions are needed. We propose

$$f''_0 = \frac{33}{5} f''_1 + \frac{56}{15h} f'_0 + \frac{288}{5h} f'_{S1} - \frac{267}{5h^2}(f_1 - f_0) - \frac{21}{5h^2}(f_2 - f_0) + \frac{7}{45h^2}(f_3 - f_0) \tag{20}$$

for the left boundary and

$$\begin{aligned} f''_N = \frac{33}{5} f''_{N-1} - \frac{56}{15h} f'_{SN+1} - \frac{288}{5h} f'_{SN} - \frac{267}{5h^2}(f_{N-1} - f_N) \\ - \frac{21}{5h^2}(f_{N-2} - f_N) + \frac{7}{45h^2}(f_{N-3} - f_N) \end{aligned} \tag{21}$$

for the right boundary with a fifth-order truncation error $-109/(16800) f_1^{(7)} h^5$. The finite difference calculation becomes to solve $2N + 3$ equations consisting of (4), (7), (8), (13), (18)–(21) to get $2N + 3$ unknown variables; f'_{Si} $(i = 0, 1, \ldots, N + 1)$ and f''_i $(i = 0, 1, \ldots, N)$. The coefficient matrix is a pentagonal system for both nonperiodic (Figure 6) and periodic boundaries, see Figure 7. Thus, the memory requirement is $5(2N + 3)$.

4. STABILITY ANALYSIS

Gustafsson *et al.* [12] developed stability analysis technique based on normal modal analysis. Their work (generally referred to as GKS theory) established conditions the inner and boundary

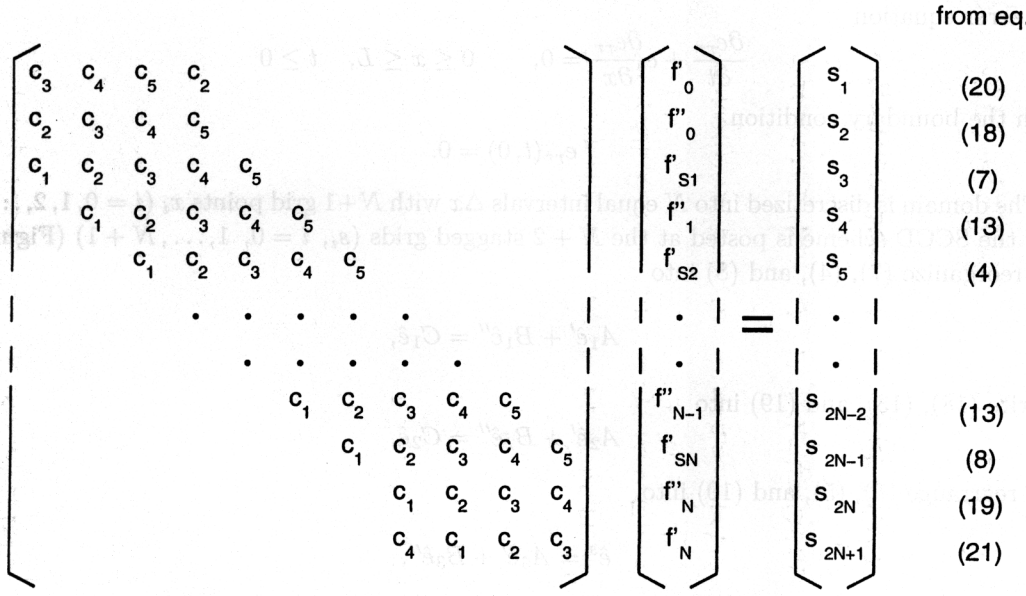

Figure 6. Coefficient matrix of the SCCD scheme for solving finite difference equation with nonperiodic boundaries.

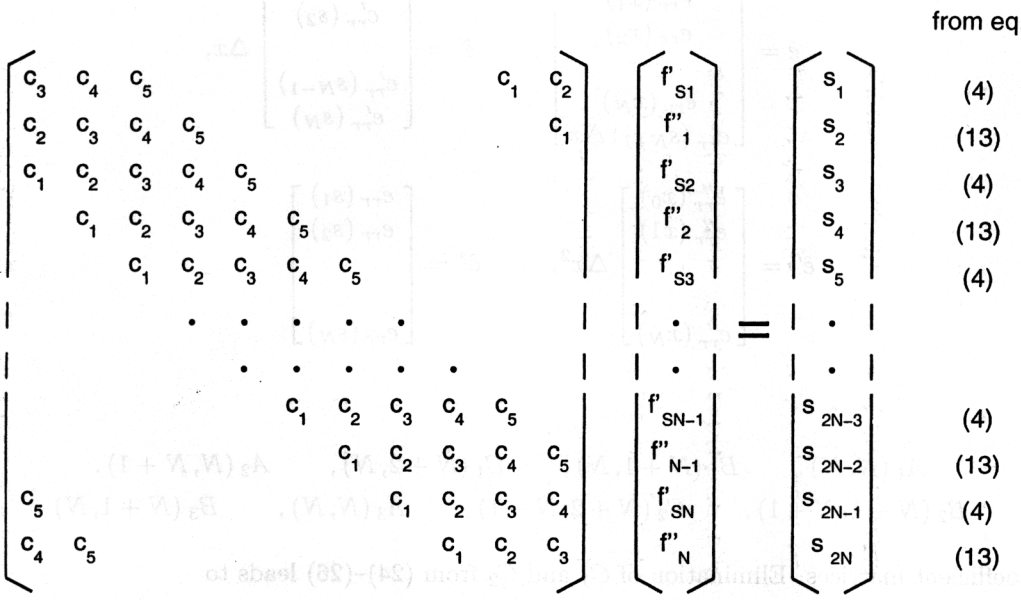

Figure 7. Coefficient matrix of the SCCD scheme for solving finite difference equation with periodic boundaries.

schemes must satisfy to ensure stability. Later on, Lele [2] and Carpenter *et al.* [3] improved the GKS technique and established a standard yardstick for acceptance of a new compact high-order scheme.

We take the Euler equation (15) with initial and boundary conditions (16) as an example for numerical stability analysis on the SCCD scheme using the eigenvalue analysis [2,3]. Define the error function by

$$e_{rr} = f - \bar{f},$$

where f and $\bar{f}$ are the exact and numerical solutions of the Euler equation (15) with the initial and boundary conditions (16). The stability of the numerical solution for (15) is the same as for

the error equation

$$\frac{\partial e_{rr}}{\partial t} + c\frac{\partial e_{rr}}{\partial x} = 0, \qquad 0 \le x \le L, \quad t \ge 0 \tag{22}$$

with the boundary condition

$$e_{rr}(t,0) = 0. \tag{23}$$

The domain is discretized into N equal intervals Δx with $N+1$ grid points x_i $(i = 0, 1, 2, \ldots, N)$ and the SCCD scheme is posted at the $N+2$ stagged grids $(s_i,\ i = 0,\ 1, \ldots, N+1)$ (Figure 1). We reorganize (7), (4), and (8) into

$$A_1\hat{e}' + B_1\hat{e}'' = C_1\hat{e}, \tag{24}$$

rewrite (18), (13), and (19) into

$$A_2\hat{e}' + B_2\hat{e}'' = C_2\hat{e}, \tag{25}$$

and rearrange (9), (5), and (10) into

$$\hat{e}^s = A_3\hat{e}' + B_3\hat{e}'', \tag{26}$$

where

$$\hat{e} = \begin{bmatrix} e'_{rr}(s_0)\,\Delta x \\ e_{rr}(x_1) \\ e_{rr}(x_2) \\ \\ e_{rr}(x_N) \\ e'_{rr}(s_{N+1})\,\Delta x \end{bmatrix}, \qquad \hat{e}' = \begin{bmatrix} e'_{rr}(s_1) \\ e'_{rr}(s_2) \\ \\ e'_{rr}(s_{N-1}) \\ e'_{rr}(s_N) \end{bmatrix} \Delta x,$$

$$\hat{e}'' = \begin{bmatrix} e''_{rr}(x_0) \\ e''_{rr}(x1) \\ \\ \\ e''_{rr}(x_N) \end{bmatrix} \Delta x^2, \qquad \hat{e}^s = \begin{bmatrix} e_{rr}(s_1) \\ e_{rr}(s_2) \\ \\ \\ e_{rr}(s_N) \end{bmatrix}$$

and

$$A_1(N,N), \quad B_1(N+1,N), \quad C_1(N+2,N), \quad A_2(N,N+1),$$
$$B_2(N+1,N+1), \quad C_2(N+2,N+1), \quad A_3(N,N), \quad B_3(N+1,N)$$

are coefficient matrices. Elimination of C_1 and C_2 from (24)–(26) leads to

$$\hat{e}' = B\hat{e}, \qquad \hat{e}^s = A\hat{e}, \tag{27}$$

where

$$B = \left(A_1 - B_1B_2^{-1}A_2\right)^{-1}\left(C_1 - B_1B_2^{-1}C_2\right), \qquad A = A_3B + B_3\left(B_2^{-1}C_2 - B_2^{-1}A_2B\right). \tag{28}$$

Substitution of (27) into (22) leads to

$$A\frac{\partial\hat{e}}{\partial t} = -\frac{c}{\Delta x}B\hat{e}. \tag{29}$$

Using the normal modes

$$\hat{e}(x,t) = \exp(\omega t)\tilde{e}(x).$$

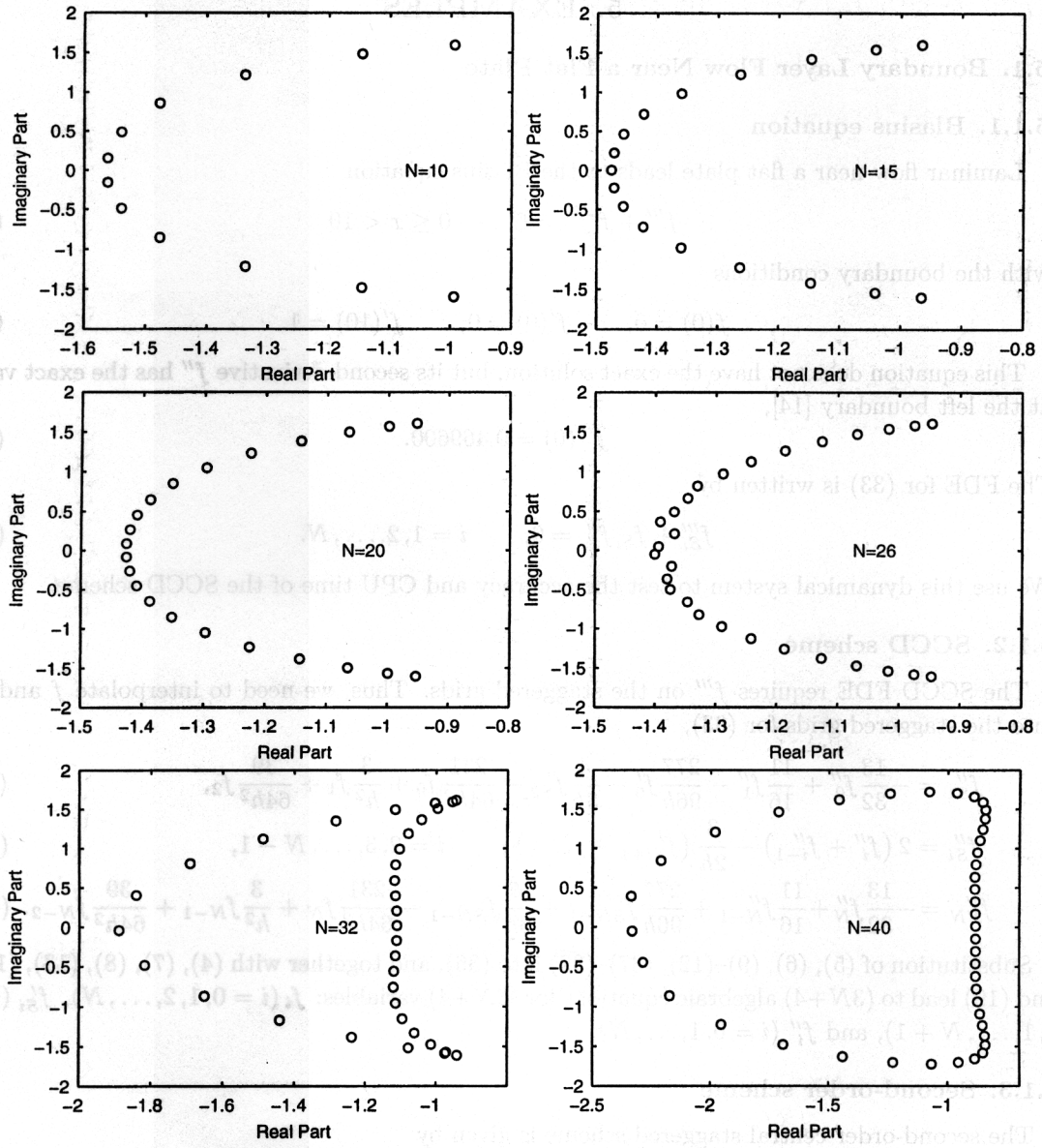

Figure 8. Eigenvalues ω'_j of equation (30) for various horizontal resolutions.

Equation (29) becomes an eigenvalue problem

$$-\frac{\omega\Delta x}{c}A\tilde{e} = B\tilde{e}, \tag{30}$$

where $\tilde{e}(x)$ is an $(N+2)$-dimensional vector. The algebraic equation (30) has $(N+2)$ eigenvalues

$$\omega'_j = \frac{\omega_j \Delta x}{c}, \qquad j = 0, 1, \ldots, N+1. \tag{31}$$

If the real part of all eigenvalues

$$\mathrm{Re}\,(\omega'_j) \le 0, \qquad j = 0, 1, \ldots, N+1, \tag{32}$$

the numerical schemes are stable.

We use the Matlab [13] built-in function 'eig' to compute the eigenvalues of (30). Figure 8 shows the eigenvalues $\{\omega'_j\}$ in the complex plane with different resolution N. All $\mathrm{Re}\,(\omega'_j)$ are negative, which indicates the stability of the SCCD scheme.

5. EXAMPLES

5.1. Boundary Layer Flow Near a Flat Plate

5.1.1. Blasius equation

Laminar flow near a flat plate leads to the Blasius equation

$$f''' + f\,f'' = 0, \qquad 0 \le x < 10 \tag{33}$$

with the boundary conditions

$$f(0) = 0, \qquad f'(0) = 0, \qquad f'(10) = 1. \tag{34}$$

This equation does not have the exact solution, but its second derivative f'' has the exact value at the left boundary [14],

$$f''(0) = 0.469600. \tag{35}$$

The FDE for (33) is written by

$$f'''_{Si} + f_{Si} f''_{Si} = 0, \qquad i = 1, 2, \ldots, N. \tag{36}$$

We use this dynamical system to test the accuracy and CPU time of the SCCD scheme.

5.1.2. SCCD scheme

The SCCD FDE requires f''' on the staggered grids. Thus, we need to interpolate f and f'' into the staggered grids for (33),

$$f''_{S1} = -\frac{13}{32} f''_0 + \frac{11}{16} f''_1 - \frac{277}{96h} f'_0 - \frac{4}{3h} f'_{S2} - \frac{231}{64h^2} f_0 + \frac{3}{h^2} f_1 + \frac{39}{64h^2} f_2, \tag{37}$$

$$f''_{Si} = 2\left(f''_i + f''_{i-1}\right) - \frac{3}{2h}\left(f'_{Si+1} - f'_{Si-1}\right), \qquad i = 2, 3, \ldots, N-1, \tag{38}$$

$$f''_{SN} = -\frac{13}{32} f''_N + \frac{11}{16} f''_{N-1} + \frac{277}{96h} f'_{SN+1} + \frac{4}{3h} f'_{SN-1} - \frac{231}{64h^2} f_N + \frac{3}{h^2} f_{N-1} + \frac{39}{64h^2} f_{N-2}. \tag{39}$$

Substitution of (5), (6), (9)–(12), (37)–(39) into (36), and together with (4), (7), (8), (13), (18), and (19) lead to $(3N+4)$ algebraic equations for $(3N+4)$ variables: f_i $(i = 0, 1, 2, \ldots, N)$, f'_{Si} $(i = 0, 1, \ldots, N+1)$, and f''_i $(i = 0, 1, \ldots, N)$.

5.1.3. Second-order scheme

The second-order central staggered scheme is given by

$$f_{Si} = \frac{f_i + f_{i-1}}{2}, \qquad i = 1, 2, \ldots, N, \tag{40}$$

$$f''_i = \frac{f_{i-1} - 2f_i + f_{i+1}}{h^2}, \qquad i = 1, 2, \ldots, N-1. \tag{41}$$

The Blasius equation (33) is discretized by

$$\frac{f''_i - f''_{i-1}}{h} + f_{Si} \frac{f''_i + f''_{i-1}}{2} = 0, \qquad i = 1, 2, \ldots, N \tag{42}$$

and the boundary conditions (34) is changed into

$$f_0 = 0, \qquad f''_0 = \frac{((f_1 - f_0)/h - f'_0)}{h/2} = \frac{f_1 - f_0}{h^2}, \tag{43}$$

$$f''_N = \frac{(f'_N - (f_N - f_{N-1})/h)}{h/2} = \frac{(1 - (f_N - f_{N-1})/h)}{h/2}. \tag{44}$$

The Blasius equation (33) with the boundary condition (34) becomes a set of nonlinear algebraic equations (40)–(44) for f_i, f''_i $(i = 0, 1, 2, \ldots, N)$, and f_{S_i} $(i = 0, 1, 2, \ldots, N+1)$.

5.1.4. Iteration

The iterative method is used to solve the nonlinear algebraic equation (36). For each step of iteration m, the variables f_{S_i} $(i = 0, 1, 2, \ldots, N+1)$ are taken the values of the previous step, $f_{Si}^{(m-1)}$. Thus, the two sets of nonlinear algebraic equations become linearized and easy to solve.

The iteration starts from a linear field,

$$f_i^{(0)} = x_i, \qquad i = 1, 2, \ldots, N,$$

which provides the first guess values for f_{S_i}

$$f_{Si}^{(0)} = \frac{x_i + x_{i-1}}{2}, \qquad i = 1, 2, \ldots, N. \tag{45}$$

The solutions of the two linearized systems lead to a set of new values $f_{Si}^{(1)}$, which are used for the next iteration. The iteration stops at the step M as

$$\left| f''^{(M)}(0) - f''^{(M-1)}(0) \right| < 10^{-9}. \tag{46}$$

5.1.5. SCCD verification

We solve the Blasius equation (33) numerically with both SCCD and second-order schemes under various horizontal resolutions and record the CPU time (a SGI origin-100 was used). Since f'' of the Blasius equation has the exact value at the left boundary (35), the accuracy evaluation between SCCD and second-order schemes is pursued using $f''(0)$. The difference between the numerical and exact values of $f''(0)$ is regarded as the computational error.

Error versus grid cell number diagram (Figure 9a) shows that for the same grid cell number, the error of the SCCD scheme is more than three orders of magnitude smaller than the second-order scheme. For example, the errors of the SCCD and the second-order schemes for the cell number 50 are 1.28×10^{-4} and 1.99×10^{-1}, an error reduction by 1555 times using the SCCD scheme. For the same accuracy, the SCCD requires much less (1–2 order of magnitudes) resolutions. For example, the grid cell number should be 10,000 (second-order scheme), or 85 (SCCD) if the error is 0.3×10^{-7}.

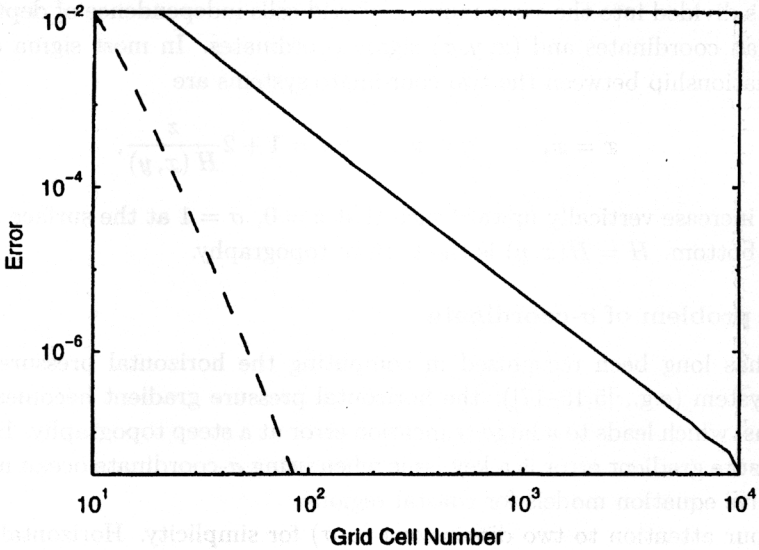

(a) Error versus grid cell number.

Figure 9. Error and CPU time comparison between SCCD (solid curve) and second-order (dashed curve) schemes.

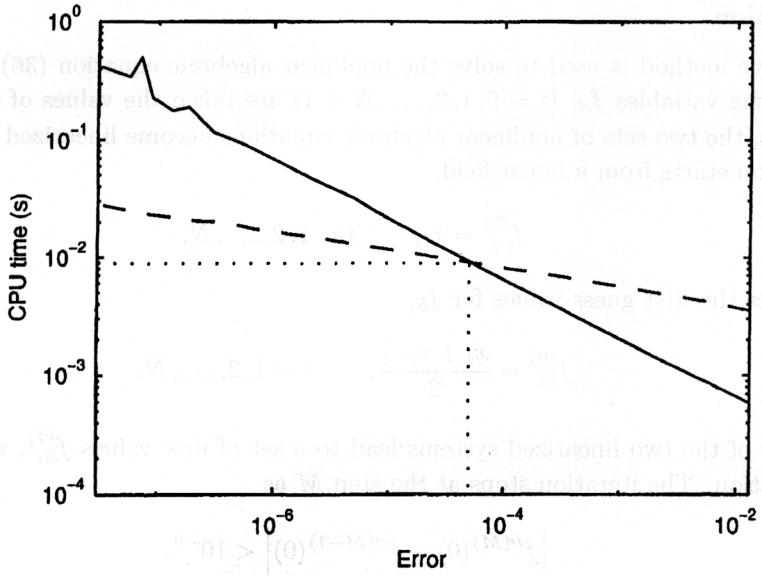

(b) CPU time versus error.

Figure 9. (cont.)

Usually, the CPU time increases with the accuracy. CPU time versus error diagram (Figure 9b) shows a more rapid increase using SCCD than the second-order scheme, and the existence of a critical error (5.01×10^{-5}), where both SCCD and second-order schemes consume the same CPU time (near 0.0088 s). For the error less (more) than this critical value, the SCCD scheme consumes more (less) CPU time.

5.2. σ-Coordinate Ocean Model

5.2.1. σ-coordinate

In coastal ocean prediction models (most staggered), the effects of bottom topography must be taken into account. This can be done by using a terrain-following σ-coordinate system, where the water column is divided into the same number of grid cells independence of depth. Let (x_*, y_*, z) denote Cartesian coordinates and (x, y, σ) sigma coordinates. In most sigma coordinate ocean models, the relationship between the two coordinate systems are

$$x = x_*, \qquad y = y_*, \qquad \sigma = 1 + 2\frac{z}{H(x,y)}, \tag{47}$$

where z and σ increase vertically upward such that $z = 0$, $\sigma = 1$ at the surface and $z = -H$ and $\sigma = -1$ at the bottom. $H = H(x, y)$ is the bottom topography.

5.2.2. Major problem of σ-coordinate

A problem has long been recognized in computing the horizontal pressure gradient in the σ-coordinate system (e.g., [5,15–17]): the horizontal pressure gradient becomes a difference between two terms, which leads to a large truncation error at a steep topography. How to reduce the horizontal pressure gradient error is a key issue when using σ-coordinate ocean models, especially of using primitive equation models for coastal regions.

We restrict our attention to two dimensions (x, σ) for simplicity. Horizontal gradients in the z- and σ-coordinates are related by

$$\frac{\partial p}{\partial x_*} = \frac{\partial p}{\partial x} + (1-\sigma)\frac{\partial H}{\partial x}\frac{1}{H}\frac{\partial p}{\partial \sigma}. \tag{48}$$

Most ocean models are hydrostatically balanced, i.e.,

$$\frac{\partial p}{\partial z} = -\rho g, \tag{49}$$

where g is the acceleration due to gravity, ρ is the density of the fluid. Substitution of (49) into (48) and use of

$$\frac{\partial}{\partial z} = \frac{2}{H}\frac{\partial}{\partial \sigma}$$

yield

$$\frac{\partial p}{\partial x_*} = \frac{\partial p}{\partial x} - \frac{1}{2}(1-\sigma)\rho g \frac{\partial H}{\partial x}, \tag{50}$$

which is used for computing the horizontal pressure gradient in the σ-coordinate ocean models. Since horizontal gradients $\frac{\partial p}{\partial x_*}$, $\frac{\partial p}{\partial x}$, and $\frac{\partial h}{\partial x}$ are evaluated at the staggered points, we have to use (5), (9), and (10) to interpolate ρ at the staggered points.

5.2.3. Seamount test case

Chu and Fan [5] used an ordinary seven-point sixth-order difference scheme to reduce the horizontal pressure gradient error. Since most ocean numerical models use three-point staggered schemes, it is hard to apply the ordinary sixth-order schemes (more than three points) to ocean models. For staggered grid ocean models, the SCCD scheme overcomes the grid mismatch. It is easy to apply SCCD to ocean models.

We use a seamount test case to illustrate the benefit of using SCCD. Suppose a seamount located inside a periodic f-plane ($f_0 = 10^{-4}\text{s}^{-1}$) channel with two solid, free-slip boundaries along constant y. The domain is a periodic channel, 320 km long and 320 km wide. The channel has a far-field depth $\eta_{\max}$ and in the center includes an isolated Gaussian-shape seamount (Figure 10) with a width W and an amplitude η_s,

$$\eta(x,y) = \eta_{\max} - \eta_s \exp\left[-\frac{(x-x_0)^2 + (y-y_0)^2}{W^2}\right], \tag{51}$$

where (x_0, y_0) are the longitude and latitude of the seamount center [5].

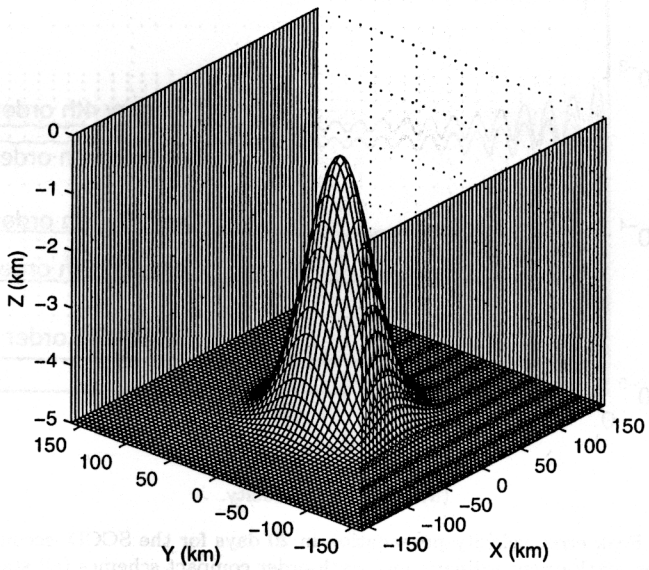

Figure 10. Seamount geometry.

The fluid is exponentially stratified and initially at rest. The initial density field has the form,

$$\rho_i = \overline{\rho}(z) + \hat{\rho}\exp\left(\frac{z}{H\rho}\right), \tag{52}$$

where z is the vertical coordinate, and $H_\rho = 1000\,\mathrm{m}$, and

$$\overline{\rho}(z) = 28 - 2\exp\left(\frac{z}{H\rho}\right) \tag{53}$$

is a reference density field. Here a constant density, $1000\,\mathrm{kg\,m^{-3}}$, has been subtracted for the error reduction. For a standard test case [5], the parameters are given by

$$W = 40\,\mathrm{km}, \quad \eta_{\max} = 5000\,\mathrm{m}, \quad \eta_s = 4500\,\mathrm{m}, \quad \hat{\rho} = 0.2\,\mathrm{kg\,m^{-3}}, \quad A_H = 10^{10}\,\mathrm{m^4\,s^{-1}}. \tag{54}$$

Unforced flow over seamount in the presence of resting, level isopycnals is an ideal test case for the assessment of pressure gradient errors in simulating stratified flow over topography. The flow is assumed to be reentrant (periodic) in the along channel coordinate (i.e., x-axis). This seamount test case has a known solution, i.e., zero velocity, after integrating from rest with no external forcing (atmospheric or lateral boundary) if there is no computational error. Another nonzero velocity generated is due to the computational error. We use this seamount case of the semispectral primitive equation model (SPEM) version 3.9 to test the new difference scheme. The reader is referred to the original reference [18] and the SPEM 3.9 User's Manual [19] for detailed information. In the horizontal directions, the model uses the staggered C-grid, second-order finite difference discretization except for the horizontal pressure gradient, which the user has choice of either second-order or fourth-order difference discretization [20]. In the vertical direction, the model uses a boundary fitted σ-coordinate system. The discretization is by spectral collocation using Chebyshev polynomials. Our model configuration is similar to that of Beckmann and Haidvogel [21]. The time step and grid size used here are

$$\Delta t = 675\ \mathrm{s}, \qquad \Delta x = \Delta y = 5\,\mathrm{km}.$$

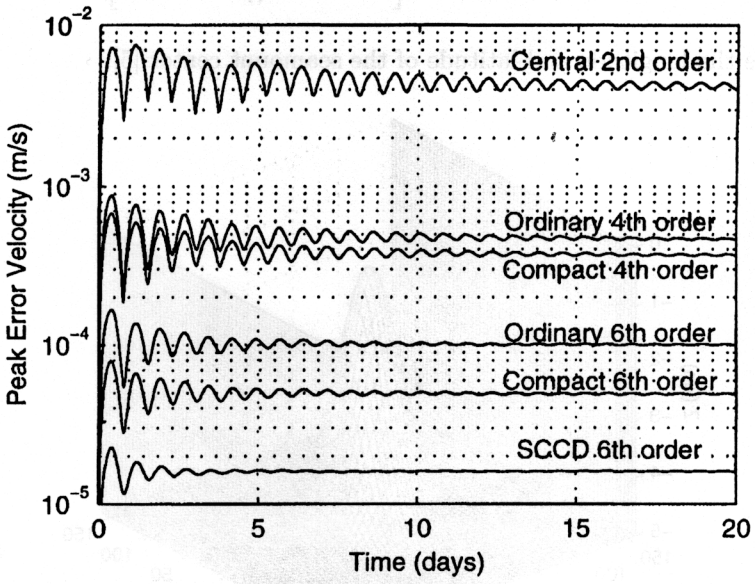

(a) Peak error velocity.

Figure 11. Peak error velocity propagation in 20 days for the SCCD, second-order, fourth-order, sixth-order ordinary, and sixth-order compact schemes (all staggered). The formulas for the compact schemes compared are listed in the Appendix.

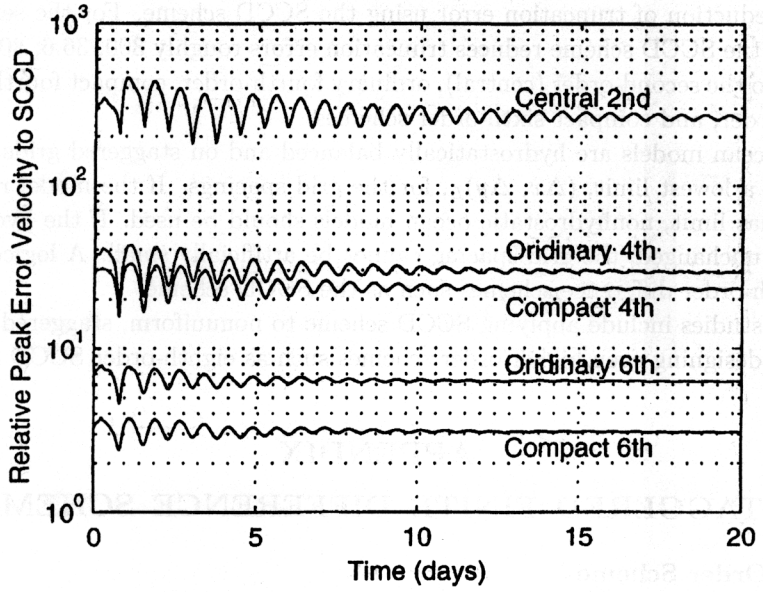

(b) Relative peak error velocity to SCCD scheme.

Figure 11. (cont.)

Owing to a very large number of calculations performed, we discuss the results exclusively in terms of the maximum absolute value the spurious velocity (called peak error velocity) generated by the pressure gradient errors. Figure 11a shows the time evolution of the peak error velocity for the first 20 days of integration with six different schemes. The formulas of these schemes are given in the Appendix. The peak error velocity fluctuates rapidly during the first few days' integration. After five days of integration, the peak error velocity show the decaying inertial oscillation superimposed into mean values: 0.4 cm/s (ordinary second-order central, three-point), 0.048 cm/s (ordinary fourth-order with five-point), 0.04 cm/s (compact fourth-order with four-point), 0.01 cm/s (ordinary sixth-order with seven-point), 0.004 cm/s (compact sixth-order with five-point), and 0.0013 cm/s (SCCD with three-point). The steady approach of the peak error velocities to these values for the six schemes indicates the stability of the computation. Also, we computed the error ratio between the existing schemes versus the SCCD scheme (Figure 11b). The errors for the second-order (central), ordinary fourth-order, compact fourth-order, ordinary sixth-order, and compact sixth-order schemes are roughly 300, 36.6, 30, 8, 3 times of the that of the three-point sixth-order SCCD scheme.

6. CONCLUSIONS

(1) From this study, it can be stated that the three-point sixth-order SCCD scheme is a promising highly accurate method for both derivative computation and FDE solutions. The advantage of this highly accurate three-point staggered scheme is its potentially wide application to geophysical computations, especially to atmospheric and oceanic numerical models.

(2) This scheme requires satisfaction of FDE not only on the interior grid points, but also on the boundary nodes.

(3) For periodic boundaries, the SCCD scheme has sixth-order accuracy at all grid points including boundary nodes. But for nonperiodic boundaries, an additional fifth-order boundary condition is needed at the boundary nodes to close the system.

(4) The eigenvalue analysis indicates the stability of the SCCD scheme.

(5) Two examples (Blasius equation and semispectral primitive equation ocean model) show

great reduction of truncation error using the SCCD scheme. For the semispectral ocean model, the SCCD scheme reduces truncation errors roughly 300, 36.6, 30, 8, 3 times compared to the second-order (central), ordinary fourth-order, compact fourth-order, ordinary sixth-order, and compact sixth-order schemes.

(6) Most ocean models are hydrostatically balanced and on staggered grids. Such a balance sets up a lowest limit, $(\Delta x, \Delta y)_L$, for the grid spacings. If the model resolution is finer than that limit, nonhydrostatic ocean models should be used. If the hydrostatic balance is kept unchanged, the grid spacing cannot be artificially small. A logical approach is to use high-order difference schemes such as the SCCD scheme.

(7) Future studies include applying SCCD scheme to nonuniform, staggered grid systems, as well as designing even higher-order schemes such as eighth-order SCCD scheme.

APPENDIX

STAGGERED FINITE DIFFERENCE SCHEMES

A1. Second-Order Scheme

The staggered second-order scheme is given by

$$\left(\frac{\partial p}{\partial x}\right)_i \simeq \frac{p_{i+1/2} - p_{i-1/2}}{h} - \frac{1}{24}\left(\frac{\partial^3 p}{\partial x^3}\right)_i h^2,$$

$$\rho_i = \frac{\rho_{i-1/2} + \rho_{i+1/2}}{2} + O\left(h^2\right).$$

A2. Fourth-Order Schemes

Ordinary scheme

The staggered fourth-order ordinary scheme is given by

$$\left(\frac{\partial p}{\partial x}\right)_i = \frac{p_{i-3/2} - 27p_{i-1/2} + 27p_{i-1/2} - p_{i+1/2}}{24h} + \frac{3}{640}\left(\frac{\partial^5 p}{\partial x^5}\right)_i h^4,$$

$$\rho_i = \frac{9}{16}(\rho_{i-1/2} + \rho_{i+1/2}) - \frac{1}{16}(\rho_{i-3/2} + \rho_{i+3/2}) + O\left(h^4\right).$$

Compact scheme

The staggered fourth-order compact scheme is given by

$$\frac{1}{24}\left[\left(\frac{\partial p}{\partial x}\right)_{i-1} + 22\left(\frac{\partial p}{\partial x}\right)_i + \left(\frac{\partial p}{\partial x}\right)_{i+1}\right] = \frac{p_{i+1/2} - p_{i-1/2}}{h} - \frac{17}{5,760}\left(\frac{\partial^5 p}{\partial x^5}\right)_i h^4$$

with

$$\rho_i = \frac{1}{2}(\rho_{i-1/2} + \rho_{i+1/2}) + \frac{1}{16}\left[\left(\frac{\partial \rho}{\partial x}\right)_{i-1} - \left(\frac{\partial \rho}{\partial x}\right)_{i+1}\right] h + O\left(h^4\right).$$

At the left boundary, we use

$$\left(\frac{\partial p}{\partial x}\right)_1 = \frac{(-(11/12)p_{1/2} + (17/24)p_{3/2} + (3/8)p_{5/2} - (5/24)p_{7/2} + (1/24)p_{9/2})}{h} - \frac{71}{1920}\left(\frac{\partial^5 p}{\partial x^5}\right)_i h^4,$$

$$\rho_1 = \frac{35}{128}\rho_{1/2} + \frac{35}{32}\rho_{3/2} - \frac{35}{64}\rho_{5/2} + \frac{7}{32}\rho_{7/2} - \frac{5}{128}\rho_{9/2} + O\left(h^4\right).$$

The right boundary point has the similar formulation.

A3. Sixth-Order Schemes

Ordinary scheme

The staggered sixth-order compact scheme is given by

$$\left(\frac{\partial p}{\partial x}\right)_i = \frac{-9p_{i-5/2} + 125p_{i-3/2} - 2,250p_{i-1/2} + 2,250p_{i+1/2} - 125p_{i+3/2} + 9p_{i+5/2}}{1920h} - \frac{5}{7,168}\left(\frac{\partial^7 p}{\partial x^5}\right)_i h^6.$$

Compact scheme

The staggered sixth-order compact scheme is given by

$$\frac{1}{80}\left[9\left(\frac{\partial p}{\partial x}\right)_{i-1} + 62\left(\frac{\partial p}{\partial x}\right)_i + 9\left(\frac{\partial p}{\partial x}\right)_{i+1}\right] = \frac{1}{240}\frac{-17p_{i-3/2} - 189p_{i-1/2} + 189p_{i+1/2} + 17p_{i+3/2}}{h} + \frac{61}{358,400}\left(\frac{\partial^7 p}{\partial x^7}\right)_i h^6,$$

with

$$\rho_i = \frac{9}{32}(\rho_{i-1/2} + \rho_{i+1/2}) + \frac{7}{32}(\rho_{i-3/2} + \rho_{i+3/2}) + \frac{9}{32}\left[\left(\frac{\partial \rho}{\partial x}\right)_{i-1} - \left(\frac{\partial \rho}{\partial x}\right)_{i+1}\right]\Delta + O\left(h^6\right).$$

At the left boundary, we use

$$\left(\frac{\partial p}{\partial x}\right)_1 h = \frac{1,627}{1,920}p_{1/2} - \frac{211}{640}p_{3/2} - \frac{59}{48}p_{5/2} + \frac{235}{192}p_{7/2} - \frac{91}{128}p_{9/2} + \frac{443}{1,920}p_{11/2} - \frac{31}{960}p_{13/2} + \frac{3,043}{107,520}\left(\frac{\partial^7 p}{\partial x^7}\right)_i h^6,$$

$$\rho_1 = \frac{231}{1,024}\rho_{1/2} + \frac{693}{512}\rho_{3/2} - \frac{1,155}{1,024}\rho_{5/2} + \frac{231}{256}\rho_{7/2} - \frac{495}{1,024}\rho_{9/2} + \frac{77}{512}\rho_{11/2} - \frac{21}{1,024}\rho_{13/2} + O\left(h^6\right).$$

The right boundary point has the similar formulation.

REFERENCES

1. Y. Adam, Highly accurate compact implicit methods and boundary conditions, *J. Comput. Phys.* **24**, 10–22, (1977).
2. S.K. Lele, Compact finite difference schemes with spectral-like resolution, *J. Comput. Phys.* **103**, 16–42, (1992).
3. M.H. Carpenter, D.G. Gottlieb and S. Abarbanel, The stability of numerical boundary treatments for compact high-order finite-difference schemes, *J. Comput. Phys.* **108**, 227–295, (1993).
4. M.H. Carpenter, D.G. Gottlieb and S. Abarbanel, Time-stable boundary conditions for finite-difference schemes solving hyperbolic systems: Methodology and application to high-order compact schemes, *J. Comput. Phys.* **111**, 220–236, (1994).
5. P.C. Chu and C. Fan, Sixth-order difference scheme for sigma coordinate ocean models, *J. Phys. Oceanogr.* **27**, 2064–2071, (1997).
6. R.S. Hirsh, Higher order accurate difference solutions of fluid mechanics problems by a compact differencing technique, *J. Comput. Phys.* **19**, 90–109, (1975).
7. S.G. Rubin and P.K. Khosla, Polynomial interpolation methods for viscous flow calculations, *J. Comput. Phys.* **24**, 217–244, (1977).

8. I.M. Navon and H.A. Riphagen, An implicit compact fourth-order algorithm for solving the shallow-water equations in conservation-law form, *Mon. Wea. Rev.* **107**, 1107–1127, (1979).
9. P.C. Chu and C. Fan, A three-point combined compact difference scheme, *J. Comput. Phys.* **140**, 370–399, (1998).
10. P.C. Chu and C. Fan, A three-point sixth-order nonuniform combined compact difference scheme, *J. Comput. Phys.* **148**, 663–674, (1999).
11. M.H. Carpenter, D.G. Gottlieb and S. Abarbanel, Stable and accurate boundary treatments for compact high-order finite difference schemes, *Appl. Num. Math.* **12**, 55–87, (1993).
12. B. Gustsfsson, H.-O. Kreiss and A. Sundstrom, Stability theory of difference approximations for mixed initial boundary value problems. II, *Math. Comput.* **26** (119), 649–686, (1972).
13. MATLAB, *Reference Guide*, Math Works, Natick, MA, (1992).
14. F.M. White, *Viscous Fluid Flow*, pp. 712, McGraw-Hill, New York, (1974).
15. J.M. Gary, Estimate of truncation error in transformed coordinate primitive equation atmospheric models, *J. Atmos. Sci.* **30**, 223–233, (1973).
16. R.L. Haney, On the pressure gradient force over steep topography in sigma coordinate ocean models, *J. Phys. Oceanogr.* **21**, 610–619, (1991).
17. G.L. Mellor, T. Ezer and L.-Y. Oey, The pressure gradient conundrum of sigma coordinate ocean models, *J. Atmos. Oceanic Technol.* **11**, 1126–1134, (1994).
18. D.B. Haidvogel, J.L. Wikin and R. Young, A semi-spectral primitive equation model using vertical sigma and orthogonal curvilinear coordinates, *J. Comput. Phys.* **94**, 151–185, (1991).
19. K. Hedstrom, *User's Manual for a Semi-Spectral Primitive Equation Ocean Circulation Model Version 3.9*, pp. 131, Rutgers University, New Jersey, (1994).
20. J.D. McCalpin, A comparison of second-order and fourth-order pressure gradient algorithms in a σ-coordinate ocean model, *Int. J. Numer. Methods Fluids* **18**, 361–383, (1994).
21. A. Beckmann and D.B. Haidvogel, Numerical simulation of flow around a tall isolated seamount. Part 1: Problem formulation and model accuracy, *J. Phys. Oceanogr.* **23**, 1736–1753, (1993).
22. W.J. Goedheer and J.H.M. Potters, A compact finite difference scheme on a non-equidistance mesh, *J. Comput. Phys.* **61**, 269–279, (1985).
23. P.M. Prenter, *Splines and Variational Method*, pp. 100–101, Wiley-Intersci., New York, (1974).
24. J.C. Strikwerda, Initial boundary value problems for the method of lines, *J. Comput. Phys.* **34**, 94–107, (1980).